Targeting ER stress in adrenocortical carcinoma: Celastrol as a novel therapeutic candidate

Biomedicine & Pharmacotherapy 197 (2026) 119156

Contents lists available at ScienceDirect

Biomedicine & Pharmacotherapy

journal homepage: www.elsevier.com/locate/biopha

Targeting ER stress in adrenocortical carcinoma: Celastrol as a novel therapeutic candidate

Aurora Schiavon [a,*], Carlotta Evaristo [a], Laura Saba [a], Jessica Petiti [b,**], Ymera Pignochino [a,c], Soraya Puglisi [a], Paola Perotti [a], Erika Messina [a], Claudia Giachino [a], Massimo Terzolo [a,1], Marco Lo Iacono [a,*,1]

[a] Department of Clinical and Biological Sciences (DSCB), University of Turin, Turin, Italy
[b] Division of Advanced Materials Metrology and Life Sciences, Istituto Nazionale di Ricerca Metrologica (INRiM), Turin, Italy
[c] Candiolo Cancer Institute, FPO-IRCCS, Candiolo, Turin, Italy

ARTICLE INFO

Keywords:
Celastrol
H295R
Spheroids
Endoplasmic reticulum stress
Oxidative stress
RNAseq

ABSTRACT

Background: Adrenocortical carcinoma (ACC) is a rare, aggressive malignancy with limited treatment options. Mitotane, the only approved drug, has modest efficacy and frequent adverse effects, underscoring the urgent need for new therapeutic approaches. Celastrol, a triterpene compound derived from traditional Chinese medicine, exhibits anti-inflammatory activity and broad anti-tumor effects, including sensitization of cancer cells to chemo- and radiotherapy.

Purpose: In this study, we investigated for the first time the anti-cancer potential of celastrol in the ACC H295R cell line.

Methods: Using different in vitro biomolecular technologies and biochemical/biophysical experiments, we evaluated celastrol's effect on ACC cells.

Results: Celastrol induced apoptosis in ACC cells and demonstrated efficacy not only in 2D monolayer cultures but also in 3D spheroid models. Importantly, it inhibited spheroid growth and disrupted pre-formed spheroids, highlighting its activity in tumor-like structures. Mechanistic analyses suggested that celastrol triggers apoptosis through induction of endoplasmic reticulum (ER) stress and oxidative stress. These findings parallel our previous observations with mitotane, which also activates the ER stress pathway via the ATF4-ATF3 axis. This partial convergence points to ER stress induction as a potential therapeutic target in ACC.

Conclusion: identifying agents capable of complementing or replacing standard therapy remains a central challenge in ACC research. Our findings suggest that celastrol is a potent bioactive compound with activity against both monolayer and 3D ACC models, offering potential translational relevance. By elucidating ER stress as a shared mechanism between celastrol and mitotane, our work supports further exploration of this pathway as a strategy to potentially improve therapeutic outcomes in ACC patients.

1. Introduction

Adrenocortical carcinoma (ACC) is an endocrine malignancy arising from the cortical layer of the adrenal gland [1]. It is a rare and aggressive cancer, with a reported annual incidence of about 1–2 cases per million [2–4]. The overall 5-year survival rate varies by stage, ranging from

Abbreviations: ACC, Adrenocortical Carcinoma; ATCC, American Type Culture Collection; CCK8, Cell Counting Kit-8; CDDP, Cisplatin; CI, Correlation Index; DdPCR, Droplet Digital PCR; DEGs, Differentially Expressed Genes; ER, Endoplasmic Reticulum; FACS, Fluorescence-Activated Cell Sorter; FDR, False Discovery Rate; GSH, Reduced Glutathione; GSSG, Oxidized Glutathione; ISR, Integrated Stress Response; MTS, 3–4,5-dimethylthiazol-2-yl-5–3-carboxymethoxyphenyl-2–4-sulfophenyl2H tetrazolium; NAC, N-Acetylcysteine; PI, Propidium Iodide; ROS, Reactive Oxygen Species; UPR, Unfolded Protein Response.

* Correspondence to: DSCB, Regione Gonzole, 10, Orbassano, TO 10043, Italy.
** Correspondence to: INRiM, Str. delle Cacce, 91, Torino, TO 10135, Italy.
E-mail addresses: aurora.schiavon@unito.it (A. Schiavon), carlotta.evaristo@unito.it (C. Evaristo), laura.saba@unito.it (L. Saba), j.petiti@inrim.it (J. Petiti), ymera.pignochino@unito.it (Y. Pignochino), soraya.puglisi@unito.it (S. Puglisi), paola.perotti@unito.it (P. Perotti), erika.messina@unito.it (E. Messina), claudia.giachino@unito.it (C. Giachino), massimo.terzolo@unito.it (M. Terzolo), marco.loiacono@unito.it (M. Lo Iacono).
[1] MLI and MT equally contributed to this manuscript.

https://doi.org/10.1016/j.biopha.2026.119156

Available online 25 February 2026

relatively favorable outcomes in localized disease to only 10–20 % in metastatic one [5–7]. Whereas surgical resection of the primary tumor with the eventual addition of adjuvant systemic therapy remains the only curative option, the recurrence rate is high (30–80 %) [8,9]. The options for patients with advanced, recurrent, or metastatic disease are limited, and they include mitotane in combination with classic chemotherapeutic agents, such as cisplatin, etoposide, and doxorubicin [10,11]. Mitotane (o,p'-DDD) is still the only drug approved for the treatment of ACC by both the U.S. Food and Drug Administration and the European Medicines Agency, despite its limited efficacy and the wide range of adverse effects that often lead to treatment discontinuation [12–16]. In this context, there is an urgent need to find new therapeutic alternatives to improve patients' outcomes.

Celastrol ($C_{29}H_{38}O_4$) is a quinone-methylated triterpenoid compound, first extracted from the root bark of *Tripterygium wilfordii* Hook F., a traditional Chinese medicine, and well known for its anti-inflammatory properties in the treatment of rheumatoid arthritis [17]. Over the past few years, studies have highlighted celastrol's multiple pharmacological activities, ranging from anti-diabetic and anti-obesity [18,19], to immunomodulatory [20], and, above all, anti-cancer activity [21]. Notably, celastrol has been reported to have a broad spectrum of anti-tumor effects on various cancer cells, such as lung, ovarian, stomach, liver, leukemia, colon, and breast cancers [22], and it has also been shown to exert an enhancing effect on cellular sensitization to radiotherapy and chemotherapy [23]. Celastrol has been shown to exert its anti-cancer potential through multiple molecular mechanisms, including inhibition of proliferation and cell-cycle arrest [24]; apoptosis, endoplasmic reticulum (ER) stress, and reactive oxygen species (ROS) production [25]; autophagy modulation [26]; inhibition of migration, invasion, and metastasis [27]. Although celastrol exhibits promising therapeutic potential, its clinical application is limited by safety concerns, including dose- and exposure-related toxicity [28]. These challenges are largely attributed to its poor water solubility, low bioavailability, and off-target effects [29]. Accordingly, substantial efforts have been directed toward developing novel formulations and advanced delivery strategies to enhance targeted delivery, improve pharmacokinetic profiles, and reduce adverse effects.

In this study, we investigated for the first time the potential anti-cancer effects of celastrol in the adrenocortical carcinoma H295R cell line, a well-established preclinical model for ACC. Our results show that celastrol induces apoptosis in ACC cells. Notably, its efficacy extends beyond monolayer cultures to 3D spheroid models, where it not only inhibits spheroid growth but also disrupts pre-formed spheroids.

2. Materials and methods

2.1. Drugs and chemicals

All the drugs and chemicals were provided by MedChemExpress LLC (Monmouth Junction, NJ 08852, USA). Celastrol (cat. #HY-13067) and cisplatin (CDDP, cat. #HY-17394) were dissolved in DMSO at final stock concentration of 22.2 mM and 33.3 mM, respectively, while mitotane (cat. #HY-13690) and etoposide (cat. #HY-13629) were dissolved in 10 mM stock solutions, and stored at −20 °C. N-Acetylcysteine (NAC, cat. #HY-B0215) was dissolved in water in 100 mM stock solution and stored at −20 °C.

2.2. Cell lines and culture conditions

H295R cells (RRID: CVCL_0458) were kindly provided by Prof. S. Sigala (Department of Molecular and Translational Medicine, University of Brescia, Italy) and cultured at 37°C with 5 % CO_2 according to American Type Culture Collection (ATCC) instructions. Media and supplements were purchased from Euroclone (Pero, Italy). H295R cells were grown in DMEM: F12 50:50 medium (Gibco: Thermo Fisher Scientific, Waltham, Massachusetts, USA) supplemented with 2.5 % NuSerum (Corning, #355100, Thermo Fisher Scientific, Waltham, Massachusetts, USA), penicillin/streptomycin (Gibco) and ITS Premix (Corning #354350). Unless indicated, all experiments were conducted in the absence of serum to minimize confounding effects on drug availability and cellular stress responses [30]. Cell lines were periodically tested for mycoplasmas and authenticated by genetic profiling through polymorphic short tandem repeat loci with the PowerPlex® 16 System (Promega, Madison, Wisconsin, USA) and Applied Biosystems 3130 Genetic Analyzer (Thermo Fisher Scientific, Waltham, Massachusetts, USA).

2.3. Sievewell slides

Sievewell™ slides (©Tokyo Ohka Kyogyo Co., Ltd) are microwell chips, composed by a main chip chamber and two side ports. The chip chamber has 370,000 hexagonal nanowells with a width of 20 μm and a depth of 25 μm, at the bottom of which there are two pores of 2 μm diameter. These pores are connected to the two side ports through a micro-gap of 3 μm diameter situated below the chip membrane. Pipetting from the side ports allows the flushing of liquids through the microwells without losing loaded cells. In fact, when cells are seeded onto the chip and the medium is aspirated from the side ports, they are pulled down and individually captured into the nanowells. To load the cells onto the Sievewell™ slides, we followed the manufacturer's procedures as described in the user guide. We used Sievewell™ slides to generate spheroids from single cells, since the small size of the pores allows for the loading of one cell per pore. This approach was adopted to reduce size heterogeneity and improve reproducibility in 3D spheroid-based drug testing.

2.4. Cell viability assay

The 3-(4,5-dimethylthiazol-2-yl)-5-(3-carboxymethoxyphenyl)-2-(4-sulfophenyl)2H tetrazolium (MTS, Promega, Madison, Wisconsin, USA) or Cell Counting Kit-8 (CCK8; HY-K0301 MedChemExpress) viability assay was performed as follows: cells were seeded in a 96-well plate (5×10^4 cells/well) and cultured for 24 h testing different drug concentrations (untreated vs. celastrol [0.2–2 μM], mitotane [3–250 μM], CDDP [10–200 μM], and etoposide [3–100 μM]); for each drug, the range of increasing concentrations was selected to maximize the sigmoidal pattern of the dose-response curve. Substrate was added after drug incubation, according to the manufacturer's instructions, including background subtraction using no-cell control wells, and the appropriate absorbance was recorded by iMark™ Microplate Absorbance Reader (Bio-Rad). Technical quadruplicates were performed for each drug condition, and the experiments were replicated at least twice. The half maximal inhibitory concentration at 24 h ($IC50_{24}$) is a measure of the effectiveness of a molecule/drug in inhibiting a specific biological or biochemical function. In our analysis, this is the concentration of a single drug (celastrol, mitotane, etoposide, and CDDP), or combinations, resulting in a 50 % reduction in cell viability after 24 h of drug exposure. $IC50_{24}$ values were calculated by evaluating the viability data using Sigmoidal Dose Response analysis with GraphPad software 8. Since $IC50_{24}$ was generated by an algorithm that depends on the starting cell number and other experimental conditions, we maintained the drug-alone condition for every replicate in each experiment.

2.5. Apoptosis analysis

To measure apoptosis, H295R cells (1×10^6 cells/well) were seeded in 6-well plates in the absence of serum; after 24 h of incubation with the appropriate concentration of drug, cells were detached with Accutase (cat. #00–4555–56, Thermo Fisher Scientific, Waltham, Massachusetts, USA) and stained with propidium iodide (PI) and FITC-Annexin V (Invitrogen). FACS analysis was performed with BD FACS Celesta (Becton Dickinson Biosciences, Franklin Lakes, New Jersey, USA).

2.6. Cell cycle analysis

H295R cells (1 $\times 10^6$ cells/well) were seeded in 6-well plates in the absence of serum; after 24 h of incubation with the appropriate concentration of celastrol, cells were detached with Accutase (Thermo Fisher Scientific) and fixed in 80 % ethanol for 30 min at room temperature (RT). Cells were further diluted and incubated for 30 min at RT with PI staining solution (PI 50 μg/ml, Tris-HCl pH 8 10 mM, $MgCl_2$ 5 mM, and RNase 10 μg/ml). Cell cycle analysis was performed by flow cytometry (FACS) with a BD FACS Celesta (Becton Dickinson Biosciences).

2.7. RNA extraction

Total RNA was extracted from cell lines, either treated or untreated with celastrol, with PRImeZOL Reagent (cat. #AN1100, Canvax, Parque Tecnológico de Boecillo, Boecillo, Valladolid, Spain), following the manufacturer's instructions. Genomic DNA contamination was removed by DNase I treatment (Promega, Madison, Wisconsin, USA). Total RNA was then quantified via NanoDrop (Thermo Fisher Scientific, Waltham, Massachusetts, USA) and stored at −80 °C.

2.8. RNA sequencing

Libraries were generated from total RNA using the Illumina TruSeq Stranded Total RNA Library Prep Gold and NovaSeq 6000 System (Illumina), following the Illumina standard procedures and kits. The fastp tool with default settings was utilized for quality control and preprocessing of FASTQ files, in order to obtain clean data for downstream analysis [31]. Subsequently, quantification of transcript expressions was generated by the Salmon algorithm (Ver 1.9.0, specific parameters: -l A -p 40 –validateMappings –seqBias –gcBias), which considers experimental attributes and biases, commonly observed in real RNAseq data, to perform inferences on transcript expressions [32]. Next, the filtered counts table was used as input to determine differential gene expression, performed using the program edgeR version 3.32.1 in R [33]. This procedure resulted in a gene list containing false discovery rate (FDR), p-value, and counts per million mapped reads (CPM). Genes with an absolute $|\log2FC| \geq 1$ (which corresponds to at least a 100 %-fold change) and FDR < 0.05 were considered differentially expressed genes (DEGs). These DEGs were used for subsequent analysis.

2.9. cDNA synthesis and droplet digital PCR (ddPCR)

2 μg of total RNA were reverse-transcribed with random hexamer primers and MultiScribe Reverse transcriptase (High-Capacity cDNA Archive Kit, Applied Biosystems: Thermo Fisher Scientific), according to the manufacturer's instructions. Different primers were designed to evaluate genes of interest (HSD3β2, HSPA6, SEL1L3, AKR1B10, and HRPT1, see Supplementary Table 1) using Primer Express 2.0 (Thermo Fisher Scientific, Waltham, MA, USA). Primer efficiency was calculated for each transcript with RT–PCR (ABI Prism 7500 Sequence Detection System; Applied Biosystems) by using serial dilutions of cDNA of H295R. The specificity of each amplicon was evaluated by analyzing the respective melting curves. The ATF4 gene transcript was evaluated with an "assay on demand" probe, purchased from Thermo Fisher Scientific (Assay ID: Hs00909569_g1). Each sample was partitioned into ~20,000 droplets by an automated droplet generator (QX200™ Droplet Generator, Bio-Rad, Hercules, CA, USA), and each droplet was amplified by using ddPCR™ Supermix (for Probes or Evagreen) (Bio-Rad, Hercules, CA, USA), following the thermal cycling conditions suggested by the manufacturer. Custom primers were used at a final concentration of 100 nM, while the ATF4 "assay on demand" was diluted following the manufacturer's instructions. After the amplification, each sample was then loaded onto the QX200™ Droplet Reader (Bio-Rad, Hercules, CA, USA), and ddPCR data were analyzed with QX Manager™ analysis software (version 2.0, Bio-Rad, Hercules, CA, USA). Each sample was analyzed at least in biological duplicates for all celastrol's concentrations in study. The target concentration in each sample was expressed and normalized as a percentage of target gene/*HRPT1* (Gene Ratio); differential expression was evaluated relative to celastrol 0 μM (untreated cell line) and expressed as $\log_2$ of fold change ($\log_2$(Gene Ratio$_{[\text{conc x}]}$/Gene Ratio$_{[0\mu M]}$)). Statistical analysis was performed using unpaired t-Tests with a significance level of $p < 0.05$, comparing each celastrol concentration versus the untreated control.

2.10. Western blot and protein analysis

To isolate total protein content, cells were lysed on ice with RIPA buffer (Thermo Fisher Scientific, Waltham, Massachusetts, USA) supplemented with Halt™ Protease and Phosphatase Inhibitors Single-Use Cocktail (Thermo Fisher Scientific, Waltham, Massachusetts, USA), and cell debris was removed by centrifugation at 16,000 × g at 4 °C for 10 min. Equal amounts of protein (70 μg) for each sample were loaded and analyzed through SDS-PAGE (Any kD™ Mini-PROTEAN® TGX™ Precast Protein Gels, Bio-Rad). Proteins were then transferred onto PVDF membranes (Trans-Blot Turbo Mini 0.2 μm PVDF Transfer Packs, Bio-Rad) using the Trans-Blot Turbo Transfer System and the protocol recommended by the producer, then blocked in EveryBlot Blocking Buffer (Bio-Rad) for 10 min and incubated overnight at 4 °C with primary antibodies (1:1000 dilution in EveryBlot Blocking Buffer, Bio-Rad) against: ATF4 (Cell Signaling Technology (CST), #11815, Danvers, MA, USA), cleaved-PARP (CST, #5625), phospho-eIF2α (CST, #3398), BiP (CST, #3177), Vinculin (CST, #13901), HSPA6 (Santa-Cruz Biotechnology, #sc-374589) and HSP70 (Santa-Cruz Biotechnology, #sc-32239). Anti-rabbit IgG/HRP (CST, #7074) and anti-mouse IgG/HRP (CST, #7076) were used as secondary antibodies (1:8000 dilution). An enhanced chemiluminescence method (Clarity ECL and Clarity Max ECL, Bio-Rad, Hercules, CA, USA) was used for protein-bound detection, and the images were acquired using the ChemiDoc™ system (Bio-Rad, Hercules, CA, USA).

2.11. Oxidized and total glutathione quantification

Cells were seeded into a white 96-well plate (5 $\times 10^4$ cells/well) in DMEM F12 or DMEM F12/NAC 5 mM, and the following day were treated with increasing concentrations of celastrol. After 24 h of incubation, cells were lysed and analyzed for reduced glutathione (GSH) and oxidized glutathione (GSSG) concentrations with the GSH/GSSG-Glo Assay Kit (Cat. #V6611, Promega, Madison, Wisconsin, USA), following the manufacturer's instructions. Luminescence values (reported as relative light units, RLU) from no-cell control wells were used to determine the background signal. For all the experimental wells, containing cells treated with test compounds, the average background luminescence was subtracted from each measured value to obtain the net RLU. The ratio of reduced glutathione (GSH) to oxidized glutathione (GSSG) was calculated separately for vehicle-control and treated cells, according to the manufacturer's instructions.

3. Results

Celastrol is a quinone methide–containing pentacyclic triterpenoid with a rigid, highly hydrophobic structure derived from a friedelane-type backbone (Fig. 1). Its reactive quinone methide moiety plays a central role in its biological activity by enabling interactions with cellular proteins. The presence of a carboxylic acid group and conjugated double bonds further contributes to its pharmacological effects. Celastrol is known for its broad-spectrum anticancer activity across various cancer cell lines [22,34]. To assess its potential cytotoxic effects in adrenocortical carcinoma, we performed a viability assay using the H295R cell model (Fig. 2A). Cells were treated with increasing concentrations of the drug for 24 h. Celastrol exhibited an $IC50_{24}$ value of

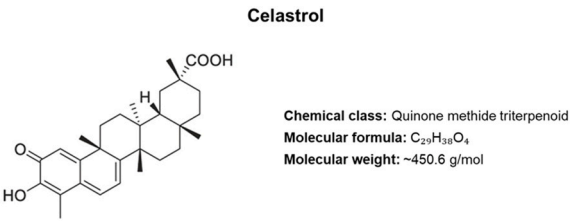

Fig. 1. *Celastrol.* Structural formula and chemical/physical characteristics of the drug.

1.63 μM [95 % confidence interval: 1.29–2.06 μM], reducing cell viability in a concentration-dependent manner. We calculated the combination index (CI) to assess potential interactions between this compound and standard therapies by co-treating H295R cells with celastrol and either cisplatin (CDDP), etoposide, or mitotane. All the experiments were performed in at least biological duplicates, and the CIs calculated for each combination are shown in Fig. 2B. The results showed no significant synergy for celastrol/etoposide and celastrol/mitotane combinations (CI 0.87 SEM ± 0.06 and CI 0.92 SEM ± 0.07, respectively). In contrast, a CI slightly over 1 was found for the celastrol/CDDP combination (CI 1.36 SEM ± 0.1), suggesting a possible antagonistic interaction under the experimental conditions tested.

To determine if celastrol-mediated cell death was associated with apoptosis in H295R cells, we performed FACS analysis with Annexin V and PI staining. The cell phenotypic/morphological changes, the cytofluorimetry graphs and related statistical analysis are shown in Supplementary Figure 1. The results of FACS analysis, expressed as percentages of total apoptotic, early apoptotic, late apoptotic, and necrotic cells, are summarized in Fig. 2C. Unlike necrotic cells, which showed no obvious fluctuations, we observed a dose-dependent increase in both early and late apoptotic cell populations following celastrol treatment. Apoptosis was also confirmed by increased expression of cleaved-PARP protein (Fig. 2D). We also conducted cell cycle analysis by FACS; however, no significant cell cycle arrest was observed 24 h after celastrol treatment (Supplementary Figure 2).

To evaluate celastrol's activity on a more complex model, we tested its cytotoxicity on 3D spheroids generated from the H295R cell line. We treated cells either during the seeding process or after spheroid formation. As shown in Fig. 3A, celastrol treatment was able to both prevent spheroid formation (in the figure indicated as "Treatment before 3D formation") and destroy the structures fully generated ("Treatment after 3D formation"). To better observe the global effect of the drug, we included in Supplementary Figure 3 representative fields for each experimental condition, acquired at lower magnification. Additionally, we evaluated the effect of celastrol on spheroids formed from single cells using SieveWell™ slides. This chip allowed us to obtain spheroids that were more homogeneous in size. As can be seen in Figs. 3B and 3C, we confirmed celastrol's efficacy both in blocking spheroids' growth at low concentrations and destroying existing spheroids. Untreated spheroids appeared translucent, while the administration of the drug, during their formation, destroyed their three-dimensional texture, making them more like cell aggregates. Furthermore, when celastrol was added to destroy the spheroids already formed, the cells still appeared compact, and the structures were no longer translucent, even if in some cases it was not able to disintegrate them due to their size.

To investigate, at the transcriptional level, the biological mechanisms affected by celastrol, we treated H295R cells for 24 h with increasing drug concentrations (0 μM, 0.5 μM and 1 μM) and performed

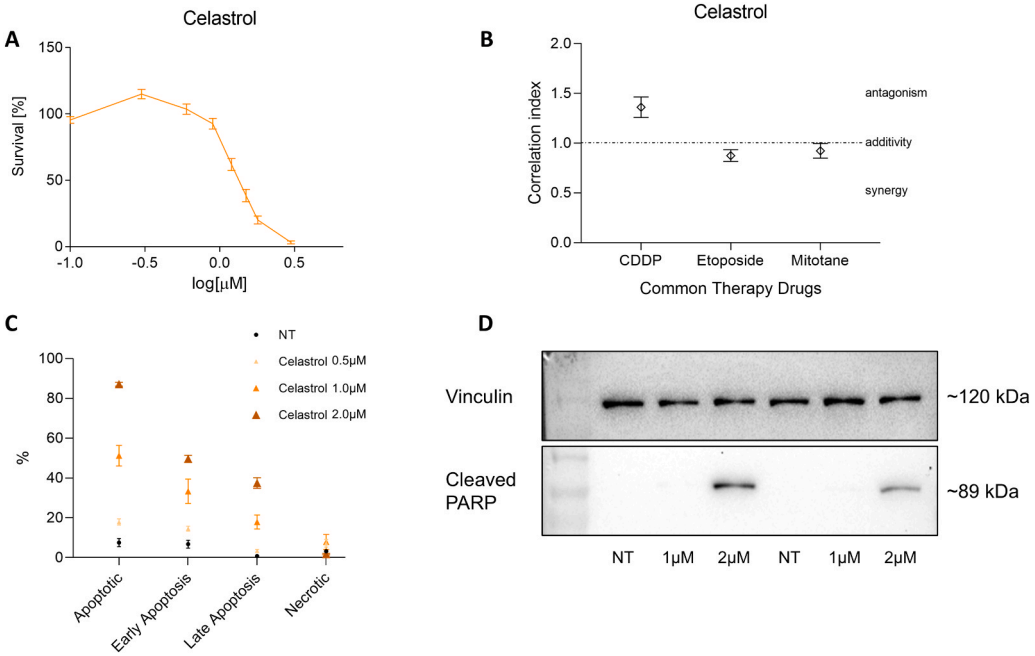

Fig. 2. *Evaluation of celastrol's cytotoxicity on H295R cell lines.* **A.** Concentration–response curve showing drug-induced inhibition of cell viability of H295R cell model. H295R cells were cultured for 24 h (h), testing different celastrol concentrations, expressed as log[μM concentration]. The range of increasing concentrations was selected to maximize the sigmoidal pattern of the dose–response graph. Celastrol exhibited an $IC50_{24}$ value of 1.63 μM [95 % confidence interval: 1.29–2.06 μM], affecting cell viability in a concentration-dependent manner. Technical quadruplicates were performed for each drug concentration, and the experiments were replicated at least twice (n ≥ 8). **B.** Correlation index (CI) analysis. H295R cells were co-treated with celastrol and either cisplatin (CDDP), etoposide, or mitotane to evaluate the possible interaction between the drugs. All the experiments were performed in at least biological duplicates (n ≥ 8). Celastrol/CDDP CI 1.36 SEM ±0.1; celastrol/etoposide CI 0.87 SEM ±0.06; celastrol/mitotane CI 0.92 SEM ±0.07. **C.** Apoptosis analysis. H295R cells were treated with celastrol (0–0.5–1–2 μM) for 24 h. Flow cytometry analysis with FITC-Annexin V/PI staining was performed to detect apoptosis. The results of the FACS analysis are expressed as percentages of total apoptotic, early apoptotic, late apoptotic and necrotic cells for each celastrol concentration. Statistical analysis described in Supplementary Figure 1. **D.** Western Blot analysis for the detection of apoptosis-related proteins. H295R cells were treated for 24 h with celastrol (0–1–2 μM). Protein lysates from each condition, in biological replicates (n = 2), were evaluated by decorating with Cleaved-PARP (49 kDa) or Vinculin (120 kDa) antibodies.

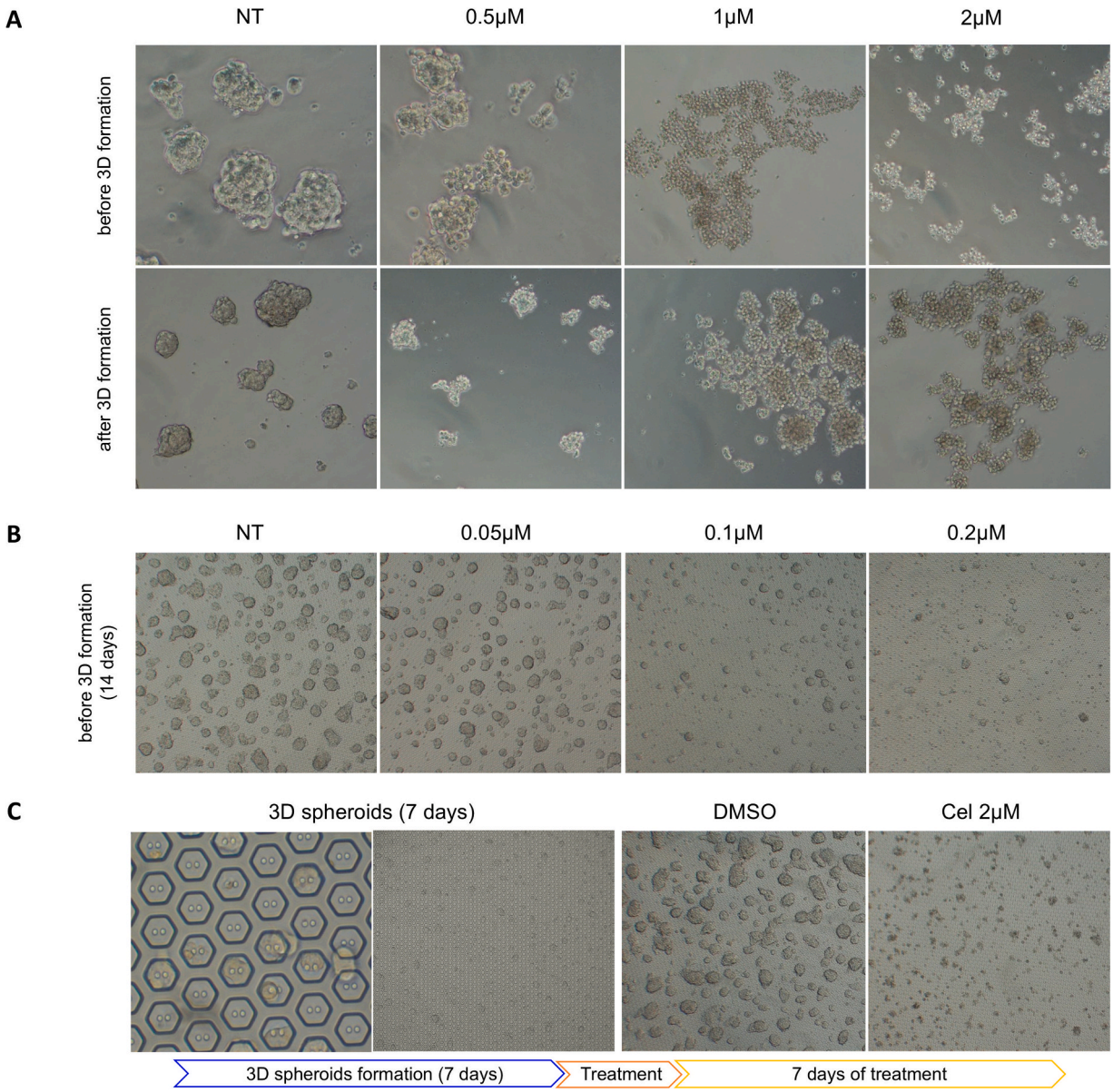

Fig. 3. *Celastrol's cytotoxicity on H295R 3D spheroids.* **A.** Brightfield microscopy images (20X magnification) of H295R spheroids treated with celastrol (0–0.5–1–2 μM) before 3D structure formation (first line) or after 3D structures formation (second line). **B.** Brightfield microscopy images (4X magnification) of H295R spheroids generated from single cells on the Sievewell™ slides. Cells were treated with different concentrations of celastrol (0–0.05–0.1–0.2 μM) during the seeding process, and after 14 days of culture, microscopy images were taken to assess the growth of the spheroids. **C.** Brightfield microscopy images (20X and 4X magnification) of H295R spheroids generated from single cells on the Sievewell slides. After their formation (7 days of culture), the spheroids were treated with celastrol 2 μM, and after 7 days of incubation, microscopy images were taken to evaluate the spheroids' celastrol-mediated disruption.

RNAseq analysis. For each celastrol concentration, we identified the DEGs compared to untreated cells. As expected, the number of DEGs rose with increasing celastrol concentration; nevertheless, the number of DEGs identified was still small. At a concentration of 0.5 μM, only two genes were significantly deregulated: FOCAD and TRIM6-TRIM34 (Supplementary Table 2), the former downmodulated (edgeR analysis: $\log_2$FC=-3.9; FDR corrected p.value=0.011) and the latter upmodulated (edgeR analysis: $\log_2$FC=5.68; FDR corrected p.value=0.038), respectively. None of these were significantly regulated at 1 μM. As shown in Fig. 4A, HSPA6 (edgeR analysis: $\log_2$FC=5.38; FDR corrected p.value<<0.01), AKR1B10 (edgeR analysis: $\log_2$FC=2.62; FDR corrected p.value=0.001) and SEL1L3 (edgeR analysis: $\log_2$FC=2.44; FDR corrected p.value=0.001) genes resulted significantly upregulated by celastrol 1 μM treatment, while HSD3B2 gene was the only transcript significantly downregulated (edgeR analysis: $\log_2$FC=-2.02; FDR corrected p.value=0.003). The regulatory pattern of these genes, at each drug concentration tested, is illustrated by the heatmap in Fig. 4B. To confirm these data, we replicated the experiments on H295R, in at least biological duplicates, and we re-evaluated the transcriptional signature using ddPCR technology. The results are presented in Fig. 4C. The deregulations observed for HSPA6 and AKR1B10 were consistent with the significant upregulation observed in the RNAseq analysis, which was mirrored by the ddPCR analysis (Fig. 4C; all unpaired t-Tests p.values <0.01). In contrast to the RNAseq analysis, for the other two genes, we obtained non-concordant results in ddPCR. In particular, the evaluation of SEL1L3 was non-significant, while that of HSD3B2 had a trend opposite to that identified in the RNAseq analysis (Fig. 4C; all $\log_2$FC<+2; all unpaired t-Tests p.value<<0.01).

Considering the biological function of the HSPA6 gene, a member of the HSP70 family, which encodes a protein chaperone with a pivotal role

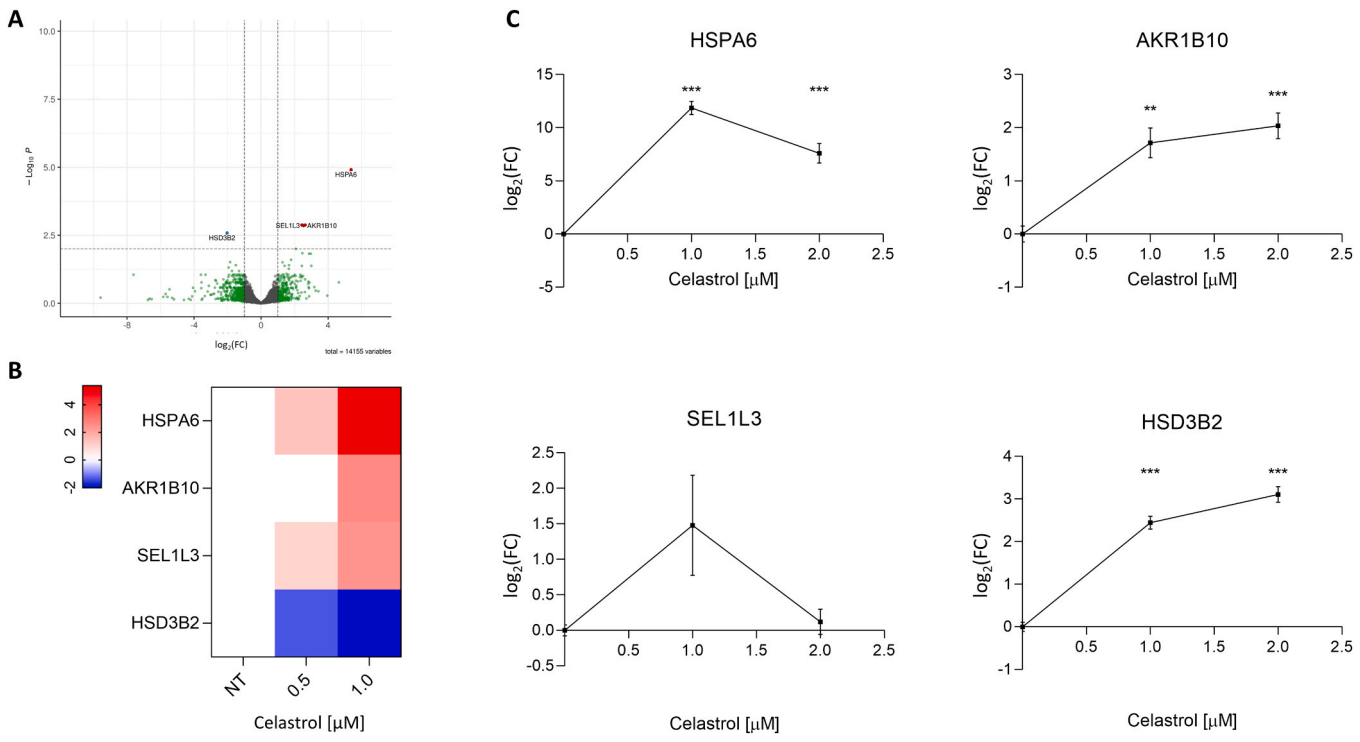

Fig. 4. *Transcriptional analysis of differentially expressed genes.* **A.** Volcano plot showing the differentially expressed genes at celastrol 1 μM compared to untreated (NT) H295R cells. HSPA6 (n = 4; log_2FC=5.38; FDR p.value <<0.01), AKR1B10 (n = 4; log_2FC=2.62; FDR p.value=0.001) and SEL1L3 (n = 4; log_2FC=2.44; FDR p.value =0.001) genes resulted significantly upregulated, while HSD3B2 gene was the only transcript significantly downregulated (n = 4; log_2FC=-2.02; FDR p.value =0.003). **B.** The heatmap shows the results of multivariate analysis using the untreated condition as "normalizer" to evaluate the tendency of gene expression across the experimental contrasts (0.5 μM/NT -> 1.0 μM/NT). **C.** ddPCR validation of the RNAseq transcriptional signature. ddPCR results were expressed as log_2 of the fold change (log_2[FC]= log_2 [Gene $Ratio_{[conc\ x]}$ /Gene $Ratio_{[0\mu M]}$). Unpaired t-Test analysis: ** indicates a p.value < 0.01; *** indicates a p.value < < 0.01.

in the protein quality control system and unfolded protein response (UPR) [35], we tested celastrol for its ability to induce ER stress. As shown in Fig. 5A, Western Blot analysis on H295R lysates showed a significant increase in HSPA6 protein at celastrol 1 μM, in accordance with RNAseq and ddPCR results. At the same concentration, we also observed an increase in ATF4 and BiP proteins compared to the untreated cells. Given the increased ATF4 protein expression observed in the immunoblot analysis, we re-evaluated the ATF4 result also at the transcriptional level using ddPCR technology. As shown in Fig. 5B, ddPCR confirmed the RNAseq analysis, in which we did not find a significant increase in ATF4 transcripts (ddPCR analysis: log_2(FC) 1 μM vs NT= 0.47; log_2(FC) 2 μM vs NT= 0.45; p.value not significant for both; RNAseq analysis: log_2(FC) 0.5 μM vs NT= -0.1384743; log_2(FC) 1 μM vs NT= -0.4, FDR not significant for both). In parallel, we detected an increase in phosphorylated eIF2α protein for celastrol 1 μM treatment (Fig. 5C).

Subsequently, we investigated celastrol's ability to induce oxidative stress by performing the GSH/GSSG-Glo assay (Promega). H295R cells were treated for 24 h with increasing concentrations of the drug alone or co-treated with N-acetylcysteine (NAC) 5 mM, a compound with known antioxidant properties [36]. We observed a significant decrease in the GSH/GSSG ratio with increasing celastrol concentration starting from celastrol 0.75 μM (Fig. 5D, orange line), indicating the induction of oxidative stress status. Instead, the GSH/GSSG ratio was almost stable in the presence of NAC (Fig. 5D, black line), which blocked celastrol's pro-oxidative activity. We also confirmed these results by CCK8 viability assay (Fig. 5E), in which we observed a preservation of H295R cell viability by NAC co-treatment, preventing the cytotoxic effect of celastrol. Furthermore, for both the GSH/GSSG ratio and cell survival assays, we compared the untreated samples for the conditions with and without NAC. We pooled all experimental data points from NAC-treated samples (black line) and compared them with NAC-untreated samples (orange line). To reduce bias from the effect of celastrol, we excluded from the NAC-untreated group any celastrol concentrations that showed a significant effect compared with the control (Fig. 5F; GSH/GSSG [0–0.50 μM] and Survival [0–0.25 μM]). We observed that NAC significantly reduced the basal oxidative stress in H295R cells (GSH/GSSG ratio increased from 16.25 to 53.17; FC=3.27; unpaired t-Tests p.value<<0.01), causing a significant boost in their proliferation (about +50 %, unpaired t-Tests p.value<<0.01). The protective effect of NAC on cells was also evident from microscopy observations. As shown in Fig. 5G, H295R cells co-treated with celastrol and NAC maintained morphological features even in the highest drug concentrations, whereas in the presence of celastrol alone, the morphological alterations were consistent with a clear cytotoxic effect.

4. Discussion

Mitotane, the only specific drug for ACC treatment, has limited activity and induces numerous side effects; therefore, mitotane treatment should be managed in specialized center, thus limiting its application, which is often questioned [13,37]. In the adjuvant setting, where treatment is given to prevent recurrence after complete tumor resection, our group recently demonstrated within the ADIUVO trial that mitotane-based therapy in patients with low-grade localized ACC does not provide a substantial benefit compared with less toxic surveillance strategies [38]. At the opposite end of the disease spectrum, in patients with advanced-stage ACC, therapeutic options remain largely unsatisfactory: mitotane has modest efficacy and conventional chemotherapy has already reached, or is close to reaching, its limits [39].

For this reason, it is necessary to intensify efforts to identify new active molecules against this orphan tumor. In this context, in this work, we focused on celastrol, a drug that has been shown to be effective against various tumors [40], often sparing the non-tumor tissue

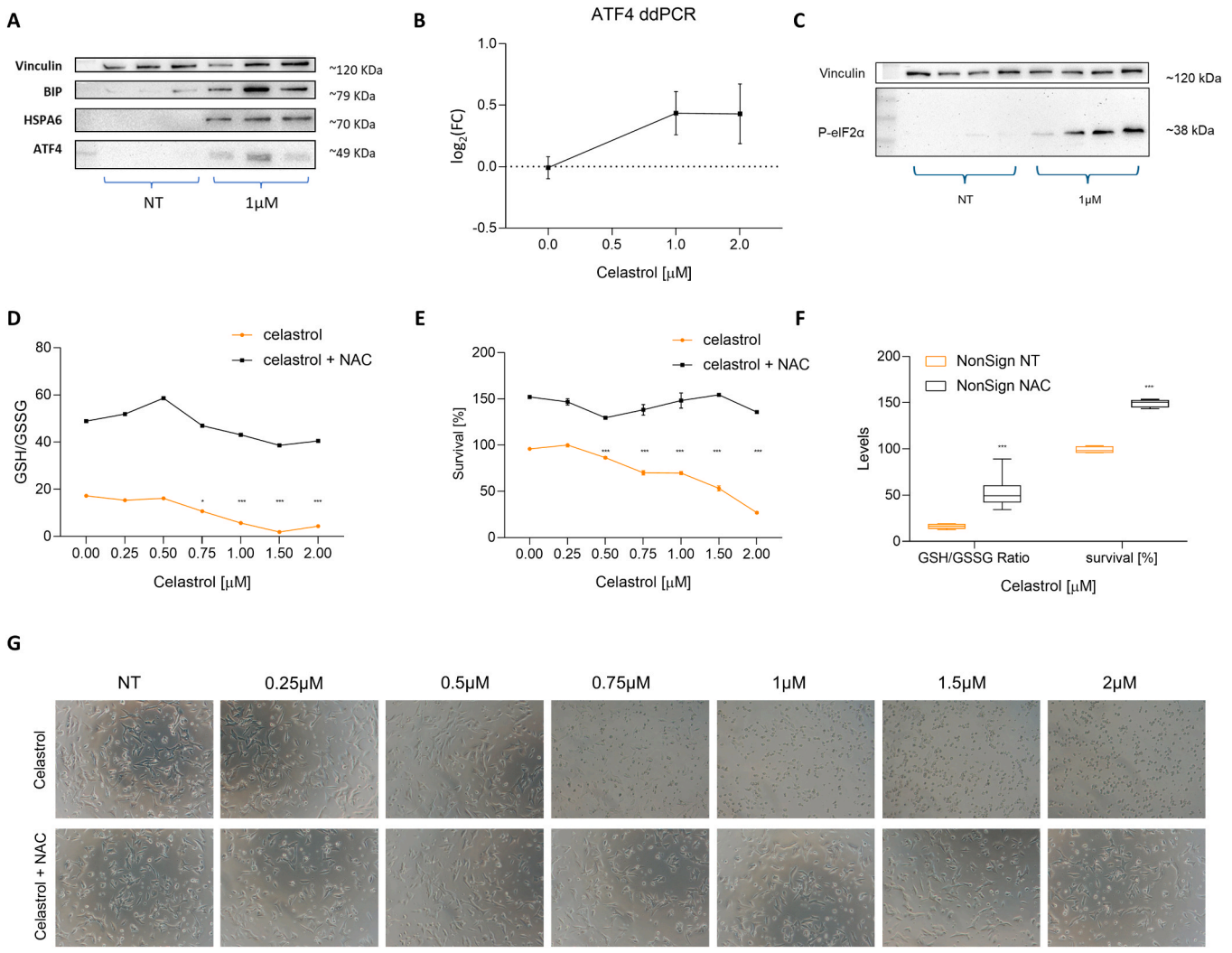

Fig. 5. *Evaluation of endoplasmic reticulum stress and oxidative stress induction.* **A.** Western blot analysis for the detection of endoplasmic reticulum stress-related proteins. H295R cells were treated for 24 h with celastrol (0–1 μM). Protein lysates from each condition, in biological triplicates (n = 3), were evaluated by decorating with HSPA6 (70 kDa), ATF4 (49 kDa), BiP (79 kDa), and Vinculin (120 kDa) antibodies. **B.** ATF4 transcript ddPCR quantification. ddPCR results were expressed as $\log_2$ of the fold change (n = 3; $\log_2$[FC]= $\log_2$ [Gene Ratio$_{[conc\ x]}$ /Gene Ratio$_{[0\mu M]}$). **C.** Western Blot analysis for the detection of phosphorylated eIF2α protein. H295R cells were treated for 24 h with celastrol (0–1 μM). Protein lysates from each condition, in biological quadruplicates (n = 4), were evaluated by decorating with p-eIF2α (38 kDa) and Vinculin (120 kDa) antibodies. **D.** Evaluation of the oxidative stress status. H295R cells were treated for 24 h with increasing celastrol concentration alone or co-treated with NAC 5 mM. The graph shows the GSH/GSSG ratio (n = 3 for each condition). **E.** CCK8 cell viability assay on H295R cells treated for 24 h with increasing celastrol concentration alone or in combination with NAC 5 mM (n = 3 for each condition). **F.** Comparison of the nonsignificant experimental point in the GSH/GSSG assay and CCK8 cell viability assay for the conditions with or without NAC (n ≥ 3 for each condition). Unpaired t-Test analysis: * indicates a p.value < 0.05; ** indicates a p.value < 0.01; *** indicates a p.value < < 0.001. **G.** Protective effect of NAC treatment on cell morphology. Brightfield microscopy images (10X) magnification of H295R cells treated with celastrol alone or in combination with NAC 5 mM.

counterpart [26,41]. Our group had previously investigated its activity for counteracting lung cancer cells' resistance to cisplatin [23]. The apoptotic mechanism of celastrol appears to vary depending on tumor cell type, involving processes such as cell cycle arrest, activation of molecular stress pathways, and increased oxidative stress [40]. However, its efficacy has not yet been tested in ACC cell lines.

In this study, we demonstrated for the first time the ability of celastrol to induce apoptosis in the ACC H295R cell model. Notably, the effect of the compound was not limited to inhibiting monolayer cell growth. In fact, celastrol effectively prevented the formation of three-dimensional structures and disrupted fully developed spheroids, leading to their regression to disorganized, necrotic-like cellular aggregates. Three-dimensional cell models have the potential to bridge the translational gap between 2D cell-based assays and human responses. They more accurately mimic the pathophysiology of human tissues, including drug penetration limitations [42]. The ability of celastrol to destroy these 3D structures, observed in our experiments, may have important implications for future patient treatment, since medical therapy usually starts when the tumor is already formed and has a three-dimensional structure. These findings should be interpreted within the limits of an *in vitro* preclinical model. Although H295R does not recapitulate the full heterogeneity of advanced or metastatic ACC, it remains the most widely used ACC cell line and uniquely allows investigation of both monolayer cultures and spontaneous 3D growth.

We observed an additive effect when celastrol was combined with etoposide and mitotane, suggesting that their pathways were not strictly overlapping. To shed light on the molecular mechanism by which celastrol induces apoptosis, we therefore performed a transcriptomic analysis, in which we found very few differentially expressed genes. Celastrol may affect multiple molecular pathways without involving specific early targets. Among the few identified, the HSPA6 transcript was the most significantly upregulated, especially at the highest

celastrol concentration. Under physiological conditions, HSPA6 acts as a molecular chaperone that promotes proper protein folding and assembly [43]. Under stress conditions, HSPA6 is involved in the degradation of misfolded polypeptides, preventing or counteracting protein aggregation, and protecting the cell from non-physiological damage [44]. This stress gene is activated in the presence of misfolded proteins and is involved in ER stress [45]. Interestingly, one of the main regulators of this pathway is ATF4, whose expression has recently been identified as a marker of poor prognosis for ACC [46]. Furthermore, our recent findings suggest that this molecular pathway may also play a key role in the pharmacological effect of mitotane [47]. However, any overlap between the two pathways does not explain the additive outcome observed when the two drugs are combined. To explore the extent of cross-talk between these mechanisms, we assessed whether a potential modulation of ATF4 transcriptional activity had previously gone undetected. Both RNAseq analysis and the subsequent ddPCR experiments confirmed that celastrol, unlike mitotane, did not transcriptionally activate ATF4. Therefore, its increase at the protein level must follow post-transcriptional events, which can be modulated by the UPR. The physiological mechanism of eIF2B supports this hypothesis. eIF2B is a critical enzyme for the mRNA-to-protein translation process in the cell, and its function is abolished by the phosphorylation of eIF2α, which causes the allosteric inhibition of eIF2B [48]. Reduction in the formation of complexes that mediate new protein synthesis triggers the Integrated Stress Response (ISR), which causes a global repression of translation initiation and a decrease in proteins synthesis. The overexpression of ATF4 is the hallmark of the ISR [49]. This effect is mediated by a post-transcriptional regulatory mechanism involving an upstream inhibitory open reading frame (ORF) that overlaps with the ORF encoding ATF4. In physiological conditions, ATF4 translation is inhibited by this ORF, but when eIF2B is blocked by p-eIF2α, the inhibitory ORF is bypassed, allowing ATF4 translation. This implies that upon eIF2α phosphorylation, the ATF4 protein is upregulated [50]. This model aligns with our results and explains why we observed no transcriptional regulation of ATF4, but an increased level of p-eIF2α in response to celastrol treatment. In addition, this molecular mechanism indirectly confirms our results on drug combinations. Indeed, although the ATF4 and endoplasmic reticulum stress pathway show a significant pharmacological role in ACC, the two drugs seem to activate it through different mechanisms. Mitotane promotes an early ATF4 transcription by triggering its molecular pathway, whereas celastrol increases ATF4 by a secondary translational pathway that involves the ISR and UPR. The combination of cellular stresses (ISR, UPR, and ER stress) ultimately results in increased oxidative stress [51]. This is consistent with our data, where the GSH/GSSG ratio was reduced by celastrol treatment, and the drug-induced apoptosis was counteracted by the co-administration of NAC. H295R cells exhibited a particularly elevated oxidative stress status, as pointed out by a low basal GSH/GSSG ratio, which was significantly improved by NAC even in untreated cells. Notably, a high baseline oxidative stress condition is frequently cited to justify the “selective” activity of celastrol on tumor cells [41,52,53]. From this perspective, adrenal tumor cells may be highly sensitive to celastrol precisely because of this basal overproduction of ROS. Our results also support this hypothesis, highlighting an increase in cell proliferation due to the co-treatment with NAC, which reduced the oxidative stress of H295R cells. These results may also explain the data obtained from the pharmacological analysis of celastrol and platinum reported in this work. Unexpectedly, unlike what we found in our lung cancer study [23], our analysis of celastrol in combination with standard ACC therapies showed that celastrol antagonized platinum-based treatment. Together, these observations indicate that the interaction between celastrol and platinum compounds is context-dependent and may vary according to the molecular background and stress-response wiring of different tumor types. A possible explanation for this mild antagonism could be a partial overlap between the two pharmacological pathways. In fact, both drugs have been associated with cell cycle arrest and increased ROS [54,55]. We did not identify significant variations in the H295R cell cycle caused by celastrol within 24 h (data not shown), and a block within this timeframe would not be consistent with the duplication time of H295R, which is at least two days [56]. On the contrary, the oxidative imbalance we observed was an early event, already visible even at low concentrations, and could justify the antagonism observed between the two drugs, which share this biological effect.

One drawback of our study is that we evaluated only one cell line, despite it being the primary reference for cellular studies on ACC. From another perspective, the H295R cell model is highly advantageous for studying ACC: it produces steroid hormones, responds to conventional therapy, and forms three-dimensional structures more physiologically similar to the tumor at diagnosis. In a previous publication, we assessed the effects of mitotane in this cell line under conditions minimizing confounding factors. This allowed us to compare the drugs’ mechanisms of action and underscored the key role of endoplasmic reticulum stress in the pharmacological treatment of ACC. Although celastrol currently has some side effects and is not ready for immediate use in ACC patients, studies of this type may suggest the evaluation of already approved drugs that share the same target.

5. Conclusion

The identification of effective active molecules to add to our therapeutic armamentarium against this rare tumor represents a major challenge for future research on ACC. Based on our findings, celastrol may be considered with interest as a potent bioactive agent in the treatment of ACC. In this scenario, this study represents the first evaluation of celastrol in ACC. Our results, although *in vitro*, are promising given that celastrol was also effective against more complex 3D structures that more physiologically mimic the tumor condition. By defining the mechanism, we have highlighted that ER stress is a key target for ACC treatment; toward with both mitotane and celastrol converge, albeit through different mechanisms. This partial overlap suggests that ER stress induction may represent a promising target for the development of new therapeutic strategies for ACC patients.

CRediT authorship contribution statement

Marco Lo Iacono: Writing – original draft, Supervision, Formal analysis, Data curation, Conceptualization. **Massimo Terzolo:** Writing – original draft, Supervision, Funding acquisition, Conceptualization. **Carlotta Evaristo:** Methodology. **Aurora Schiavon:** Writing – original draft, Methodology, Investigation, Formal analysis, Conceptualization. **Jessica Petiti:** Writing – original draft, Methodology, Investigation, Conceptualization. **Laura Saba:** Writing – original draft, Methodology, Investigation. **Soraya Puglisi:** Data curation. **Ymera Pignochino:** Methodology, Formal analysis. **Erika Messina:** Data curation. **Paola Perotti:** Data curation. **Claudia Giachino:** Methodology, Data curation.

Funding sources

This work was supported by Associazione Italiana per la Ricerca sul Cancro (AIRC), grant number IG2019-23069 to Massimo Terzolo. JP is supported by GenomeMET Project (grant no.: 22HLT06), funded by European Partnership on Metrology, co-financed by the European Union’s Horizon Europe Research and Innovation Programme and by the Participating States.

Declaration of Competing Interest

The authors stated explicitly that there are no conflicts of interest. The funders had no role in the design of the study; in the collection, analyses, or interpretation of data; in writing of the manuscript; or in the decision to publish the results.

Appendix A. Supporting information

Supplementary data associated with this article can be found in the online version at doi:10.1016/j.biopha.2026.119156.

Data Availability

The data that support the findings of this study are available from the corresponding author upon reasonable request.

References

[1] T. Else, A.C. Kim, A. Sabolch, V.M. Raymond, A. Kandathil, E.M. Caoili, S. Jolly, B. S. Miller, T.J. Giordano, G.D. Hammer, Adrenocortical carcinoma, Endocr. Rev. 35 (2) (2014) 282–326.

[2] T.M.A. Kerkhofs, R.H.A. Verhoeven, J.M. Van der Zwan, J. Dieleman, M. N. Kerstens, T.P. Links, L.V. Van de Poll-Franse, H.R. Haak, Adrenocortical carcinoma: a population-based study on incidence and survival in the Netherlands since 1993, Eur. J. Cancer 49 (11) (2013) 2579–2586.

[3] J. Pedersen, A.E. Jarlov, A.K. Rasmussen, K. Stochholm, Incidence, treatment, and survival of adrenocortical carcinoma in Denmark 2003-2019, J. Endocr. Soc. 8 (3) (2024).

[4] V. Balderrama-Brondani, A.M. Grif, T.J. Owen, K.W. Merriman, B.B. Chahla, J. Varghese, C. Jimenez, S.G. Waguespack, P.H. Graham, N.D. Perrier, S.B. Fisher, J.A. Karam, A.Y. Shah, M. Campbell, M.M. Hassan, M.A. Habra, Incidence and geographical distribution of adrenocortical carcinoma: retrospective analysis of a state cancer registry, Endocr. Pract. 30 (1) (2024) 25–30.

[5] M. Fassnacht, S. Johanssen, M. Quinkler, P. Bucsky, H.S. Willenberg, F. Beuschlein, M. Terzolo, H.H. Mueller, S. Hahner, B. Allolio, G. German, Adrenocortical Carcinoma Registry, T. European Network for the Study of Adrenal, Limited prognostic value of the 2004 International Union Against Cancer staging classification for adrenocortical carcinoma: proposal for a Revised TNM Classification, Cancer 115 (2) (2009) 243–250.

[6] M. Daher, J. Varghese, S.K. Gruschkus, C. Jimenez, S.G. Waguespack, S. Bedrose, L. Altameemi, H. Bazerbashi, A. Naing, Subbiah, M.T. Campbell, A.Y. Shah, M. Zhang, R.A. Sheth, J.A. Karam, C.G. Wood, N.D. Perrier, P.H. Graham, J.E. Lee, M.A. Habra, Temporal trends in outcomes in patients with adrenocortical carcinoma: a multidisciplinary referral center experience (vol 107, pg 1239, 2022), J. Clin. Endocr. Metab. 107 (8) (2022). E3544-E3544.

[7] S. Puglisi, A. Calabrese, F. Ferrau, M.A. Violi, M. Lagana, S. Grisanti, F. Ceccato, C. Scaroni, G. Di Dalmazi, A. Stigliano, B. Altieri, L. Canu, P. Loli, R. Pivonello, E. Arvat, V. Morelli, P. Perotti, V. Basile, P. Berchialla, S. Urru, C. Fiori, F. Porpiglia, A. Berruti, A. Pia, G. Reimondo, S. Cannavo, M. Terzolo, New findings on presentation and outcome of patients with adrenocortical cancer: results from a national cohort study, J. Clin. Endocrinol. Metab. 108 (10) (2023) 2517–2525.

[8] M. Fassnacht, S. Puglisi, O. Kimpel, M. Terzolo, Adrenocortical carcinoma: a practical guide for clinicians, Lancet Diabetes Endocrinol. 13 (5) (2025) 438–452.

[9] A. Calabrese, S. Puglisi, C. Borin, V. Basile, P. Perotti, A. Pia, P. Berchialla, M. Volante, C. Fiori, F. Porpiglia, A. Veltri, G. Reimondo, M. Terzolo, The management of postoperative disease recurrence in patients with adrenocortical carcinoma: a retrospective study in 106 patients, Eur. J. Endocrinol. 188 (1) (2023).

[10] W.M. Lo, C.M. Kariya, J.M. Hernandez, Operative management of recurrent and metastatic adrenocortical carcinoma: a systematic review, Am. Surg. 85 (1) (2019) 23–28.

[11] M. Fassnacht, O.M. Dekkers, T. Else, E. Baudin, A. Berruti, R. de Krijger, H.R. Haak, R. Mihai, G. Assie, M. Terzolo, European Society of Endocrinology Clinical Practice Guidelines on the management of adrenocortical carcinoma in adults, in collaboration with the European Network for the Study of Adrenal Tumors, Eur. J. Endocrinol. 179 (4) (2018) G1–G46.

[12] D.M. Schaap, E.X. Jie, T.G. Mayberry, B.C. Cowan, M.R. Wakefield, Y.J. Fang, Therapeutic frontiers in adrenocortical carcinoma: from standards to innovation, Med Oncol. 42 (8) (2025).

[13] M. Bianchini, G. Puliani, A. Chiefari, M. Mormando, R. Lauretta, M. Appetecchia, Metabolic and endocrine toxicities of mitotane: a systematic review, Cancers (Basel) 13 (19) (2021).

[14] V. Basile, S. Puglisi, A. Calabrese, A. Pia, P. Perotti, A. Berruti, G. Reimondo, M. Terzolo, Unwanted hormonal and metabolic effects of postoperative adjuvant mitotane treatment for adrenocortical cancer, Cancers (Basel) 12 (9) (2020).

[15] I.D. Vodanovic, A. Barac Nekic, L. Sambula, K. Zibar Tomsic, T. Dusek, D. Kastelan, Adverse events of adjuvant mitotane treatment for adrenocortical carcinoma, Endocr. Res 50 (1) (2025) 50–56.

[16] X. Wang, J. Li, Y. Zhang, R. Huang, P. Zhang, H. Hu, Comprehensive analysis of mitotane-related adverse events using the food and drug administration adverse event reporting system, Endocr. Pr. 31 (3) (2025) 278–285.

[17] K. Chen, X. Chen, S. Huang, L. Zhou, X. Zhou, Y. Lu, Z. Feng, Therapeutic effects and mechanisms of Tripterygium wilfordii extracts in rheumatoid arthritis: a systematic review and meta-analysis of preclinical studies, Sci. Rep. 15 (1) (2025) 27960.

[18] S.H. Xu, Y.Q. Feng, W.S. He, W. Xu, W. Xu, H.J. Yang, X.Y. Li, Celastrol in metabolic diseases: Progress and application prospects, Pharm. Res. 167 (2021).

[19] J.L. Liu, J. Lee, M.A.S. Hernandez, R. Mazitschek, U. Ozcan, Treatment of obesity with celastrol, Cell 161 (5) (2015) 999–1011.

[20] S.H. Venkatesha, S. Dudics, B. Astry, K.D. Moudgil, Control of autoimmune inflammation by celastrol, a natural triterpenoid, Pathog. Dis. 74 (6) (2016).

[21] J. Song, G.N. He, L. Dai, A comprehensive review on celastrol, triptolide and triptonide: Insights on their pharmacological activity, toxicity, combination therapy, new dosage form and novel drug delivery routes, Biomed. Pharm. 162 (2023).

[22] C. Wang, S. Dai, X.T. Zhao, Y.F. Zhang, L.H. Gong, K. Fu, C. Ma, C. Peng, Y.X. Li, Celastrol as an emerging anticancer agent: current status, challenges and therapeutic strategies, Biomed. Pharm. 163 (2023).

[23] M. Lo Iacono, V. Monica, T. Vavala, M. Gisabella, S. Saviozzi, E. Bracco, S. Novello, M. Papotti, G.V. Scagliotti, ATF2 contributes to cisplatin resistance in non-small cell lung cancer and celastrol induces cisplatin resensitization through inhibition of JNK/ATF2 pathway, Int. J. Cancer 136 (11) (2015) 2598–2609.

[24] X.J. Li, H.M. Wang, J. Ding, S.Z. Nie, L. Wang, L.L. Zhang, S.D. Ren, Celastrol strongly inhibits proliferation, migration and cancer stem cell properties through suppression of Pin1 in ovarian cancer cells, Eur. J. Pharm. 842 (2019) 146–156.

[25] B. Ren, H. Liu, H. Gao, S.T. Liu, Z.H. Zhang, A.M. Fribley, M.U. Callaghan, Z.X. Xu, Q.H. Zeng, Y.L. Li, Celastrol induces apoptosis in hepatocellular carcinoma cells via targeting ER-stress/UPR, Oncotarget 8 (54) (2017) 93039–93050.

[26] X.H. Liu, P.Y. Zhao, X.J. Wang, L. Wang, Y.J. Zhu, Y.D. Song, W. Gao, Celastrol mediates autophagy and apoptosis via the ROS/JNK and Akt/mTOR signaling pathways in glioma cells (vol 38, 184, 2019), J. Exp. Clin. Canc Res. 38 (2019).

[27] M.Q. Huang, L. Chen, X.Y. Ma, H.Q. Xu, Celastrol attenuates the invasion and migration and augments the anticancer effects of olaparib in prostate cancer, Cancer Cell Int. 24 (1) (2024).

[28] H. Yang, D. Chen, Q.C. Cui, X. Yuan, Q.P. Dou, Celastrol, a triterpene extracted from the Chinese "Thunder of God Vine," is a potent proteasome inhibitor and suppresses human prostate cancer growth in nude mice, Cancer Res. 66 (9) (2006) 4758–4765.

[29] J. Shi, J. Li, Z. Xu, L. Chen, R. Luo, C. Zhang, F. Gao, J. Zhang, C. Fu, Celastrol: a review of useful strategies overcoming its limitation in anticancer application, Front. Pharm. 11 (2020) 558741.

[30] A. Schiavon, L. Saba, G. Catucci, J. Petiti, S. Puglisi, C. Borin, G. Reimondo, G. Gilardi, C. Giachino, M. Terzolo, M. Lo Iacono, Albumin/mitotane interaction affects drug activity in adrenocortical carcinoma cells: smoke and mirrors on mitotane effect with possible implications for patients' management, Int. J. Mol. Sci. 24 (23) (2023).

[31] S. Chen, Y. Zhou, Y. Chen, J. Gu, fastp: an ultra-fast all-in-one FASTQ preprocessor, Bioinformatics 34 (17) (2018) i884–i890.

[32] R. Patro, G. Duggal, M.I. Love, R.A. Irizarry, C. Kingsford, Salmon provides fast and bias-aware quantification of transcript expression, Nat. Methods 14 (4) (2017) 417–419.

[33] M.D. Robinson, D.J. McCarthy, G.K. Smyth, edgeR: a Bioconductor package for differential expression analysis of digital gene expression data, Bioinformatics 26 (1) (2010) 139–140.

[34] A. Salminen, M. Lehtonen, T. Paimela, K. Kaarniranta, Celastrol: molecular targets of Thunder God Vine, Biochem. Biophys. Res. Commun. 394 (3) (2010) 439–442.

[35] S. Gupta, A. Deepti, S. Deegan, F. Lisbona, C. Hetz, A. Samali, HSP72 protects cells from ER stress-induced apoptosis via enhancement of IRE1alpha-XBP1 signaling through a physical interaction, PLoS Biol. 8 (7) (2010) e1000410.

[36] G. Aldini, A. Altomare, G. Baron, G. Vistoli, M. Carini, L. Borsani, F. Sergio, N-Acetylcysteine as an antioxidant and disulphide breaking agent: the reasons why, Free Radic. Res. 52 (7) (2018) 751–762.

[37] M. Terzolo, M. Fassnacht, A. Berruti, C. Ronchi, Navigating uncertainty in adjuvant mitotane therapy, Endocr. Pr. 31 (7) (2025) 975–976.

[38] M. Terzolo, M. Fassnacht, P. Perotti, R. Libe, D. Kastelan, A. Lacroix, W. Arlt, H. R. Haak, P. Loli, B. Decoudier, H. Lasolle, M. Quinkler, M. Haissaguerre, O. Chabre, P. Caron, A. Stigliano, R. Giordano, M.C. Zatelli, I. Bancos, M. Fragoso, L. Canu, M. Luconi, S. Puglisi, V. Basile, G. Reimondo, M. Kroiss, F. Megerle, S. Hahner, O. Kimpel, T. Dusek, S. Nolting, I. Bourdeau, V. Chortis, M.H. Ettaieb, D. Cosentini, S. Grisanti, E. Baudin, P. Berchialla, F. Bovis, M.P. Sormani, P. Bruzzi, F. Beuschlein, J. Bertherat, A. Berruti, Adjuvant mitotane versus surveillance in low-grade, localised adrenocortical carcinoma (ADIUVO): an international, multicentre, open-label, randomised, phase 3 trial and observational study, Lancet Diabetes Endocrinol. 11 (10) (2023) 720–730.

[39] M. Fassnacht, M. Terzolo, B. Allolio, E. Baudin, H. Haak, A. Berruti, S. Welin, C. Schade-Brittinger, A. Lacroix, B. Jarzab, H. Sorbye, D.J. Torpy, V. Stepan, D. E. Schteingart, W. Arlt, M. Kroiss, S. Leboulleux, P. Sperone, A. Sundin, I. Hermsen, S. Hahner, H.S. Willenberg, A. Tabarin, M. Quinkler, C. de la Fouchardiere, M. Schlumberger, F. Mantero, D. Weismann, F. Beuschlein, H. Gelderblom, H. Wilmink, M. Sender, M. Edgerly, W. Kenn, T. Fojo, H.H. Muller, B. Skogseid, F.-A.S. Group, Combination chemotherapy in advanced adrenocortical carcinoma, N. Engl. J. Med. 366 (23) (2012) 2189–2197.

[40] Y. Zhu, Y. Meng, J. Zhang, R. Liu, S. Shen, L. Gu, Y.K. Wong, A. Ma, X. Chai, Y. Zhang, Y. Liu, J. Wang, Recent Trends in anti-tumor mechanisms and molecular targets of celastrol, Int. J. Biol. Sci. 20 (14) (2024) 5510–5530.

[41] X. Chen, Y. Zhao, W. Luo, S. Chen, F. Lin, X. Zhang, S. Fan, X. Shen, Y. Wang, G. Liang, Celastrol induces ROS-mediated apoptosis via directly targeting peroxiredoxin-2 in gastric cancer cells, Theranostics 10 (22) (2020) 10290–10308.

[42] Y. Zhou, F. Yu, M. Guo, Y. Tang, Q. Xu, Bridging the gap: the role of 3D cell cultures in mimicking tumor microenvironment for enhanced drug testing accuracy, Front. Bioeng. Biotechnol. 13 (2025) 1498141.

[43] J. Radons, The human HSP70 family of chaperones: where do we stand? Cell Stress Chaperon. 21 (3) (2016) 379–404.

[44] D. Kennedy, K. Mnich, A. Samali, Heat shock preconditioning protects against ER stress-induced apoptosis through the regulation of the BH3-only protein BIM, Febs Open Bio 4 (2014) 813–821.
[45] B.H. Song, S.Y. Shen, S.Y. Fu, J.J. Fu, HSPA6 and its role in cancers and other diseases, Mol. Biol. Rep. 49 (11) (2022) 10565–10577.
[46] K. Wu, Y. Jia, Y. Li, J. Liang, S. Liu, Y. Zhu, X. Liu, X. Li, Z. Liu, Comprehensive analysis of an ATF/CREB family-based signature with regard to prognosis and immune feature in adrenocortical carcinoma: a cohort study, Int. J. Surg. (2025).
[47] A. Schiavon, L. Saba, C. Evaristo, J. Petiti, Y. Pignochino, G. Ferrero, G. Giordano, C. Tucciarello, S. Puglisi, G. Reimondo, M. Terzolo, M. Lo Iacono, Mitotane activates ATF4/ATF3 axis triggering endoplasmic reticulum stress in adrenocortical carcinoma cells, Biomed. Pharm. 184 (2025) 117917.
[48] A.M. Bogorad, K.Y. Lin, A. Marintchev, Novel mechanisms of eIF2B action and regulation by eIF2alpha phosphorylation, Nucleic Acids Res. 45 (20) (2017) 11962–11979.
[49] G. Neill, G.R. Masson, A stay of execution: ATF4 regulation and potential outcomes for the integrated stress response, Front. Mol. Neurosci. 16 (2023).
[50] R.C. Wek, Role of eIF2α kinases in translational control and adaptation to cellular stress, Csh Perspect. Biol. 10 (7) (2018).
[51] N. Chaudhari, P. Talwar, A. Parimisetty, C.L. d'Hellencourt, P. Ravanan, A molecular web: endoplasmic reticulum stress, inflammation, and oxidative stress, Front. Cell Neurosci. 8 (2014).
[52] V. Sosa, T. Moliné, R. Somoza, R. Paciucci, H. Kondoh, M.E. LLeonart, Oxidative stress and cancer: an overview, Ageing Res. Rev. 12 (1) (2013) 376–390.
[53] Z. Zhao, Y. Wang, Y. Gong, X. Wang, L. Zhang, H. Zhao, J. Li, J. Zhu, X. Huang, C. Zhao, L. Yang, L. Wang, Celastrol elicits antitumor effects by inhibiting the STAT3 pathway through ROS accumulation in non-small cell lung cancer, J. Transl. Med. 20 (1) (2022) 525.
[54] S. Dasari, P.B. Tchounwou, Cisplatin in cancer therapy: molecular mechanisms of action, Eur. J. Pharm. 740 (2014) 364–378.
[55] H. Moreira, A. Szyjka, K. Paliszkiewicz, E. Barg, Prooxidative activity of celastrol induces apoptosis, DNA damage, and cell cycle arrest in drug-resistant human colon cancer cells, Oxid. Med. Cell Longev. 2019 (2019) 6793957.
[56] W.E. Rainey, K. Saner, B.P. Schimmer, Adrenocortical cell lines, Mol. Cell Endocrinol. 228 (1-2) (2004) 23–38.